Journal of the European Ceramic Society 16 (1996) 453–465

0955-2219(95)00125-5
0955-2219/96/$15.00

Impedance Spectroscopy of Mg-Partially Stabilized Zirconia and Cubic Phase Decomposition

E. N. S. Muccillo[a] & M. Kleitz[b]

[a]Instituto de Pesquisas Energéticas e Nucleares, Comissão Nacional de Energia Nuclear, CP 11049, Pinheiros, 05422-970, S. Paulo, SP, Brazil
[b]Laboratoire d'Ionique et d'Electrochimie du Solide de Grenoble, INPG, CNRS, UJF, BP 75, 38402, St Martin d'Hères, France

(Received 3 April 1995; revised version received 30 June 1995; accepted 14 July 1995)

Abstract

Electrical conductivity measurements were carried out by impedance spectroscopy on nominally pure and magnesia-doped zirconia in the 3–13·7 mol% concentration range. In the partial-stabilization field, the impedance diagrams show the characteristic grain and grain boundary semicircles, as well as an extra arc at intermediate frequencies. This extra arc is interpreted as a characteristic of partial blocking of electrolyte conduction by the monoclinic grains. As usual, the resistances associated with the blocking processes exhibit activation energies slightly higher than the bulk resistance. All these activation energies increase with the MgO content. The cubic phase decomposition can easily and accurately be monitored by impedance spectroscopy.

1 Introduction

Recently, the electrical behaviour of a 13·7 mol% MgO-fully stabilized zirconia (Mg-FSZ) ceramic was characterized by impedance spectroscopy.[1] Electrical conduction through the grains and the blocking effect at the grain boundaries have similar characteristics to those of yttria-fully stabilized zirconia (YSZ) when the microstructures are similar.

For technological applications, MgO-partially stabilized zirconias (Mg-PSZ) are favoured because of their better mechanical properties.[2,3] Mechanical and microstructural properties of compositions in the 8–10 mol% MgO range have been extensively described in the literature. On the other hand, relatively few investigations have dealt with their electrical properties.[4,5] Conductivity values at 1000°C of 2·43 and 0·017 S m^{-1} have been reported,[4,5] respectively, for 8·2 and 9 mol% MgO.

Below 1100°C, Mg-PSZ can be a mixture of up to five crystallographic phases: cubic (c), tetragonal (t), monoclinic (m), orthorhombic (o) and the δ-phase ($Mg_2Zr_5O_{12}$). In general, the c, t and m phases are the main components. The phase diagram shows an eutectoid point at ~13·5 mol% and 1400°C. The metastable cubic solid solutions undergo a decomposition reaction with a maximum rate at ~1200 °C.[6] The destabilization of hyper- as well as hypo-eutectoid compositions has been studied, with emphasis on its effect on the material's mechanical properties.[7–11]

This study is focused on the electrical conductivity of various Mg-PSZ ceramics. For comparison, results[1] recently reported on a fully-stabilized composition of 13·7 mol% MgO will be included in some of the tables and figures. To obtain more data which could support the interpretations of the blocking effects, the conductivity and permittivity of nominally pure zirconia (NPZ) have also been evaluated with the same measurement technique. A conclusion of this work is that the presence of monoclinic zirconia can be detected and characterized by impedance spectroscopy. The decomposition of cubic zirconia could therefore be monitored by this technique. Exploratory measurements were carried out to confirm this conclusion.

2 Experimental Procedures

The starting materials were powders of ZrO_2 with impurity contents lower than 1% (Merck and DK-2 type from Zirconia Sales) and analytical reagent grade MgO (Merck). Mg-PSZ and Mg-FSZ pellets of 0·92 to 0·95 cm diameters and 0·13 to 0·16 cm thicknesses were prepared by wet mixing, pressing, sintering at 1650°C for 2 h and machining. NPZ pellets were prepared from both ZrO_2 powders by uniaxial and isostatic pressing without any high temperature heat treatment.

The apparent densities of the sintered specimens

were determined by the hydrostatic method and their phase contents by X-ray diffraction analysis. In the PSZ, the monoclinic phase content was calculated from the ratio of appropriate diffraction peaks, following the procedure recommended by Porter and Heuer.[12] Specimens for the electron microprobe analyses were polished to 1 μm. For electron microscopy, they were either fractured or polished and thermally etched. Magnesium content was checked by neutron activation analysis.

For electrical measurements, platinum electrodes (Demetron A308) were painted on the pellet bases and baked at 800°C for 15 h. The impedance measurements were performed from 5 Hz to 13 MHz with an HP 4192A impedancemeter. The results were analysed in impedance mode, using software developed for the Hydro Quebec Research Center. The Mg-PSZ diagrams were measured over the 270–700°C temperature range. Data were collected during heating and cooling cycles.

The reversible monoclinic–tetragonal (m↔t) phase transformation of the NPZ samples was studied by thermal cycling between 800 and 1370°C. Heating and cooling rates were 8·3 and 2·8°C min^{-1}, respectively. The Mg-FSZ and Mg-PSZ phase destabilization experiments were carried out at 1100°C for different annealing times, up to 14 h. In this case, the impedance diagrams were measured at a lower temperature of 553°C.

3 Physical, Chemical and Microstructural Characterizations

Table 1 shows the impurity contents of the Merck ZrO_2 powder determined by spectrographic analysis. The particle size was in the 10–40 μm range. Results for the other powders have already been published.[1] The relative density of the sintered Mg-PSZ pellets was evaluated to be ~85%, with pore sizes $\leq$0·5 μm. The density of the pressed NPZ samples was 60% of the theoretical value.

The MgO contents of the samples, as determined by neutron activation, are listed in Table 2. Solid mixtures may present some degree of chemical heterogeneity.[13] Such a non-homogeneous distribution of the solute is shown in the micrograph of the Mg X-ray image of the ZM5 sample (Fig. 1). The Mg-PSZ samples are also heterogeneous in terms of grain sizes. Figure 2 is a representative micrograph (ZM2 sample) showing two distinct regions of dissimilar grain sizes. Such bimodal distributions are found in biphasic ceramics when the phases have different grain growth rates. The larger grains have a higher MgO content, and the porosity is preferentially located within them and at the triple junctions. The small grains have a more homogeneous size distribution, as shown in the micrograph of the fractured surface of the ZM1 sample (Fig. 3).

The main difference among the Mg-PSZ samples is the relative fraction of the large to small

Table 1. Metallic impurity content of pure zirconia powder from Merck

Element	*Fe*	*Ti*	*Si*	*Ca*	*K*
Content (ppm)	< 50	< 500	< 200	< 500	< 50

Table 2. MgO content and monoclinic phase volume fractions (V_m) in sintered specimens

Specimen	*MgO content (mol%)*	V_m *(%)*
ZM1	3·16	>90
ZM2	5·14	62
ZM3	6·82	57
ZM4	8*	51
ZM5	11·89	16
ZM6	13·7	0

*Nominal concentration fixed by preparation.

Fig. 1. X-ray image showing Mg distribution for ZM5 sample.

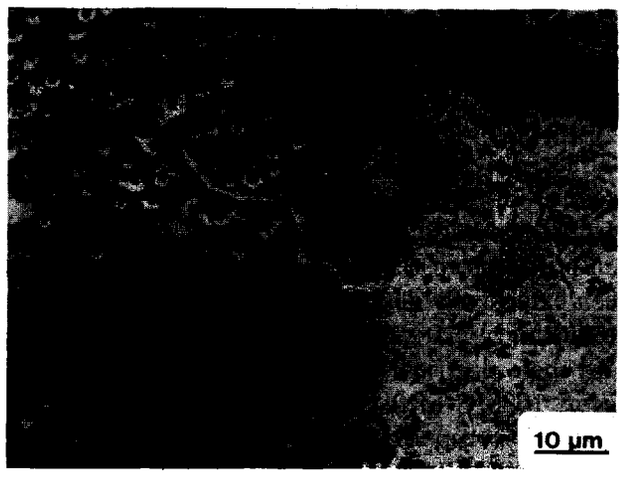

Fig. 2. Scanning electron micrograph showing zones with different grain sizes for ZM2 sample.

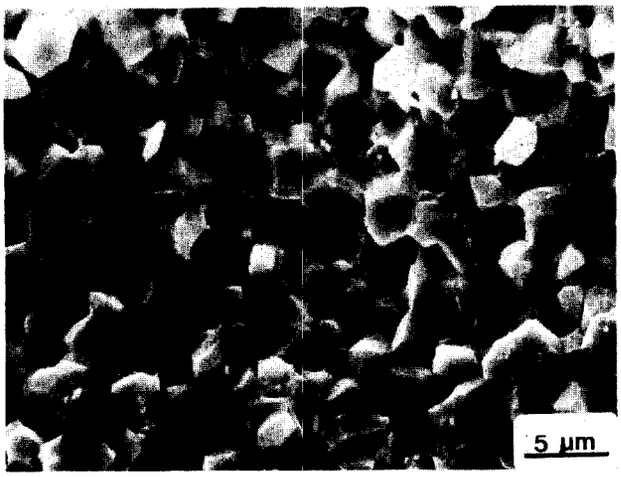

Fig. 3. Fractured surface for ZM1 sample.

grains. Increasing the magnesium content increases the fraction of large grains. The fully stabilized cubic sample has an homogeneous microstructure of rather large grains of 18 μm average size. This is consistent with a frequent observation that cubic grains have a grain growth larger than the other common phases. All the Mg-PSZ samples exhibit these chemical and microstructural heterogeneities to various extents.

The volume fractions V_m of the monoclinic phase shown in Table 2 were determined after the electrical measurements, to take into account a possible extra destabilization during the processing of the electrodes. As an example of such an alteration, Fig. 4 shows two X-ray diffractograms obtained with a sample of a composition similar to ZM4 but sintered only for 1 h at 1650°C. A

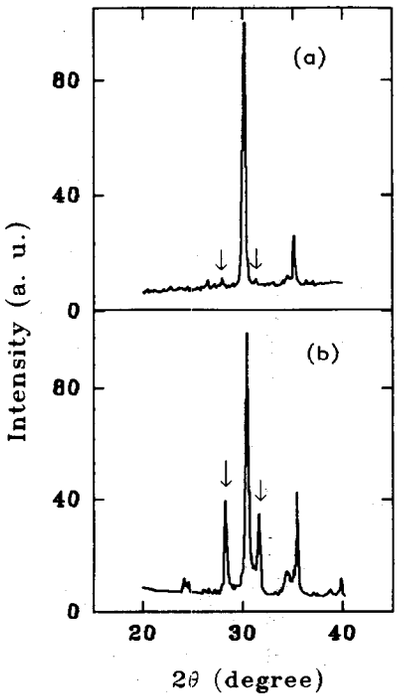

Fig. 4. X-ray diffractograms of 8 mol% MgO zirconia, sintered at 1650°C for 1 h: (a) as-sintered and (b) after measurements. The arrows point to monoclinic lines.

significant increase in the intensities of the main monoclinic phase reflections is clearly seen in the 'after measurement' profile (b) with respect to the 'as fired' profile (a). The corresponding t→m phase transformation most likely occurred during the electrode heat treatment. The absence of any hysteresis effect during the measurement temperature cycling ensures that this phenomenon did not occur during our measurements. The temperature range was lower than that of the electrode curing.

4 Electrical Conductivity and Blocking Effects of Mg-PSZ

For the sake of clarity, the electrode characteristics have been subtracted from the experimental diagrams. This could be done without ambiguity. As reported previously, the impedance diagrams of fully stabilized zirconia [ZM6, Fig. 5(a)] shows two well separated semicircles typical of the grains (g) and grain boundaries (gb), with characteristic parameters similar to those of cubic YSZ. The partially stabilized zirconias give more complex diagrams, as shown in Figs 5(b) and 5(c) (ZM5 and ZM4 samples) in which similar components can still be detected, referring to the relaxation frequencies. In the intermediary frequency domain between these conventional high and low frequency

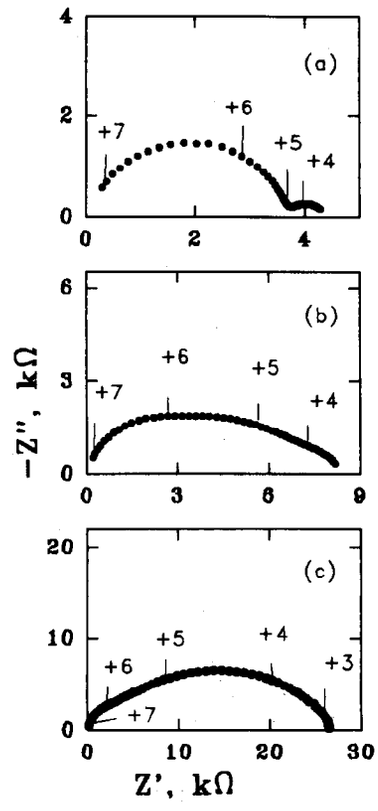

Fig. 5. Typical impedance diagrams for: (a) ZM6; (b) ZM5; and (c) ZM4 samples. T = 507°C. (Note that the axis scales are different.) The figures indicate the decimal logarithm of the measuring frequencies.

semicircles, which can also be assigned to the grains and grain boundaries for reasons given below, a third arc hereafter referred to as the extra arc (or ex) can be separated. Its contribution to the overall (or d.c.) electrolyte resistivity markedly increases with the decrease in MgO content. It dominates in the ZM1 and ZM2 impedance spectra. Because of this strong correlation, this extra arc has been ascribed to the electrical effect of the monoclinic grains, the concentration of which also varies markedly with the MgO content (Table 2). The pores, which have a relatively high concentration in the samples, certainly induce a blocking effect as well, but the reported results unambiguously show that their contribution is not dominant. Their concentration is fairly constant and should not induce highly variable effects. A further quantitative argument in favour of this statement will be given below.

For technical applications, the overall electrolyte resistivity is a key parameter. For all the investigated compositions, it was calculated from the resistance measured at the low frequency real axis intersection of the impedance diagrams. Figure 6 shows the Arrhenius plots of the corresponding resistivities ρ. As expected, these overall resistivities decrease with the increase in MgO concentration but, surprisingly enough, there is no sharp transition and no maximum at the phase boundary between the pure cubic material (ZM6) and the biphasic partially stabilized compounds. This rather smooth evolution is illustrated in Fig. 7 which shows the variations of the overall resistivities as a function of the MgO content, at 500°C. The apparent activation energies deduced from the Arrhenius diagrams of Fig. 6 also vary in a rather continuous manner as a function of the

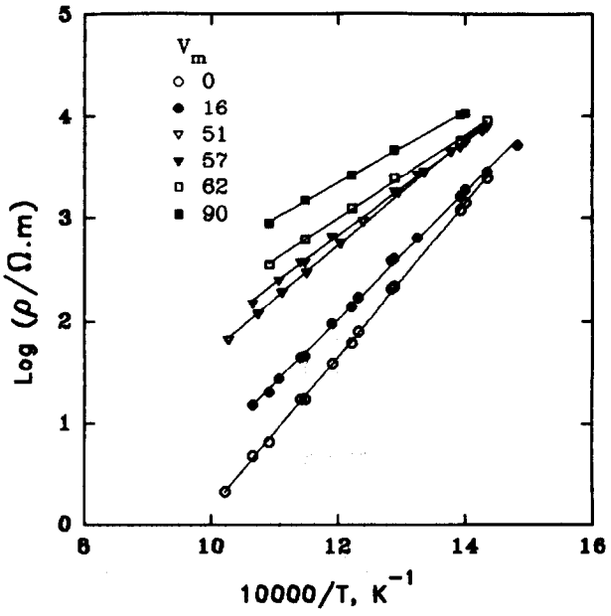

Fig. 6. Arrhenius plots of d.c. resistivities of investigated samples.

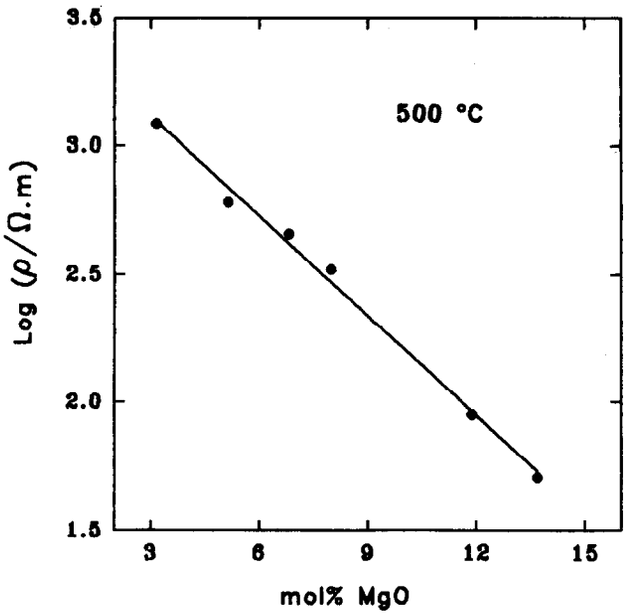

Fig. 7. Variations of resistivities at 500°C with MgO concentration.

MgO content (Fig. 8). Similar observations have already been made by Ioffe *et al.*[14] and Badwal[15] on the Y_2O_3–ZrO_2 and Sc_2O_3–ZrO_2 systems. For the Mg-PSZ compositions, in the temperature range of this investigation, the only available literature data (59 kJ mol^{-1}) were obtained with a 9 mol% MgO sample prepared from a high-silica content zirconia powder.[5] Under such conditions, magnesium silicate could have formed at the grain boundaries, thereby depleting the Mg inside the grains. In addition, the measurements were carried out at a fixed 10 kHz frequency. In zirconia-based solid solutions, the frequency distribution of the electrolyte relaxation processes (and of the electrodes) shifts towards higher frequencies with

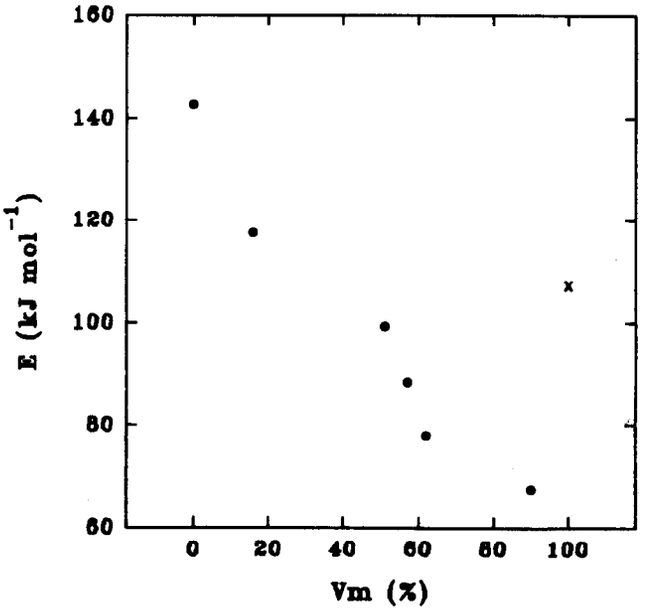

Fig. 8. Variations of d.c. resistivity apparent activation energies with monoclinic phase volume fraction V_m. The 100% point (×) is that of pure zirconia.

increasing temperature.[16,17] Therefore, measurements at a fixed frequency may give erroneous activation energies, with too low values. In the 1200–1600°C temperature range, Janke & Fischer[18] determined an activation energy of 65 kJ mol^{-1} for the 6 mol% composition.

As evident in the examples given in Fig. 5, resolution of the diagrams of our Mg-PSZ samples was not always straightforward. Note that when the ratio of the relaxation frequencies of two adjoining semicircles is of the order of 10, the overlapping is such that any resolution is questionable. Conversely, a ratio of 1000 results in an unambiguous separation. Our diagram analysis was restricted to the 350–570°C temperature range, where the fitting accuracy was good (see below). As an example of results of our resolutions, Figs 9(a) and 9(b) present the Arrhenius diagrams of the relaxation frequencies and resistivities of the ZM4 sample. The fitted straight lines are approximately parallel and the experimental scatter is small. Similar parallelism observations were also made in Mg-FSZ[1] and YSZ[19] ceramics. With this ZM4 sample, the values for the relaxation frequency ratios f_g/f_{ex} and f_{ex}/f_{gb} are ~35 and 40 (f_g, f_{ex} and f_{gb} are, respectively, the relaxation frequencies of the grain, the extra arc and the grain boundary

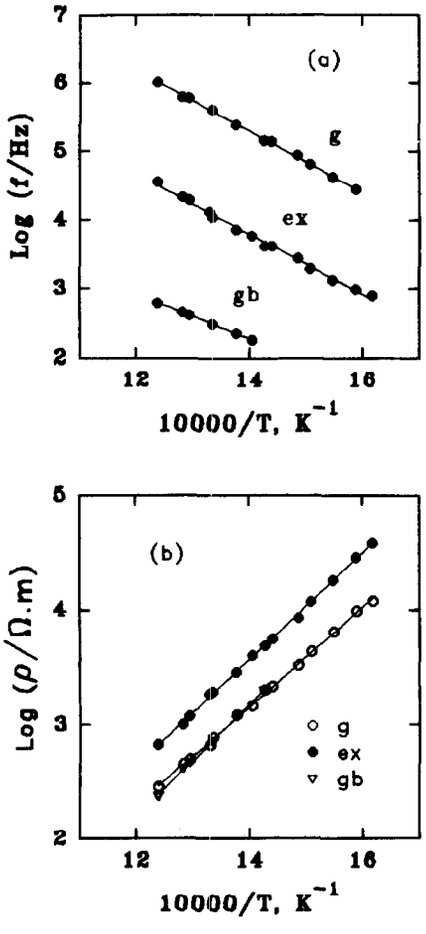

Fig. 9. Arrhenius diagrams of relaxation frequencies (a) and resistivities (b) of the three semicircles for ZM4 sample.

semicircles). The f_g/f_{ex} ratio monotonically shifts towards lower values with increasing Mg concentrations, thus increasing the overlapping.

The first feature to be ascertained in the resolution was the shape of the extra arc. For better insight concerning the possible variations in the shape of this component, the resolution was performed by successive individual fittings and subtractions. In all the resolutions we performed, the extra component did appear to be a semicircle. To test the quality of the resolution, we referred to the following criteria, as well as the coherence of the results, which will be presented below:

- the absence of any significant 'structure' in the differences between the experimental results and the fitted curves; and
- the values of the permittivity deduced from the semicircle fitting the grain response.

Figure 10 shows a typical difference diagram between the experimental results and the corresponding fitted curve (ZM4 sample, 507°C). No significant 'structure' can in fact be detected in such a diagram.

Figure 11 shows the average permittivities that were calculated for the grain semicircles of all the samples. These values are very close to the values reported in the literature[1] for the fully stabilized compositions, at temperatures similar to those of our experiments, and under conditions for which there was no ambiguity in the curve fitting. The experimental scatter of these values is also low. The values show a significant decrease as the content in the monoclinic phase increases. This is consistent with the theoretical expectation, assuming that at high temperature the permittivity of the

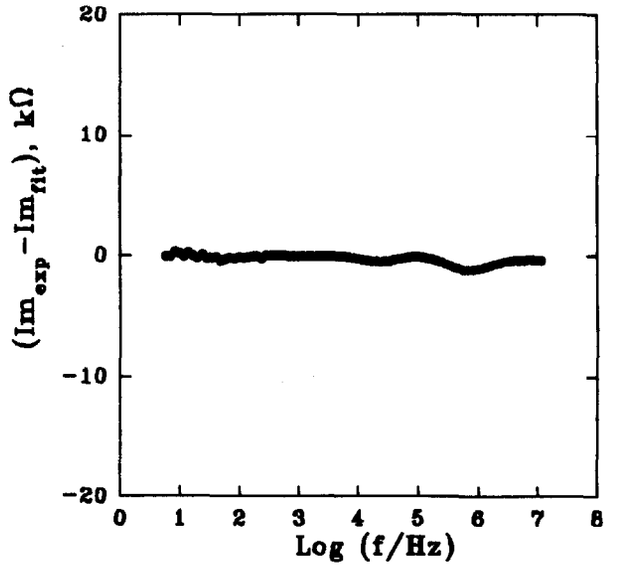

Fig. 10. Example of a difference plot between experimental (exp) and fitted (fit) values of the impedance imaginary part for ZM4 sample. T = 507°C. (The corresponding impedance moduli are of the order of 10 kΩ.)

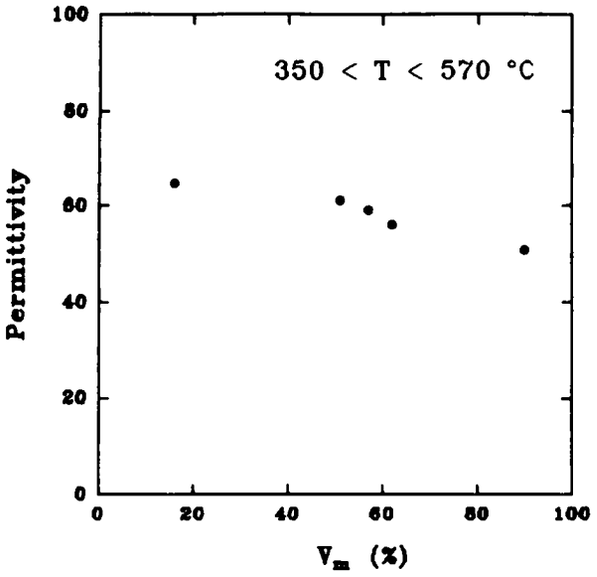

Fig. 11. Average relative permittivity deduced from the high frequency semicircle as a function of monoclinic volume fraction V_m.

monoclinic phase remains smaller than that of the other phases. At room temperature, the values are 29·3, 39·8 and 12·5, respectively, for the cubic, tetragonal and monoclinic phases.[21] A highly similar behaviour was observed[20] for Al_2O_3–YSZ composites in which the relative permittivity is 12 for the alumina grains and 55 for the YSZ grains.

The other supporting features that the resolutions revealed include:

- The Arrhenius diagrams of the relaxation frequencies of the three semicircles are almost parallel for each MgO composition, as mentioned for the ZM4 sample (see Fig. 9). This is a general observation[22] which has been made with various 'blockers' in YSZ.
- The depression angles are ~13 and 16–18°, respectively, for the grain and grain boundary responses, which are usual values. For the extra arc it is around 24°. This high value indicates a rather broad distribution of the determining blocker parameters (such as the size of the monoclinic grains).
- The resistivites that can be deduced from the extra arc and the grain boundary semicircle obey Arrhenius laws. For most compositions, the corresponding activation energies are slightly higher than those of the grains (Table 3). This is also a general observation. The relatively low precision of some of the grain boundary parameters is mainly due to the small size of the corresponding semicircles. The trend reported above for the d.c. resistivities is the same here: the activation energy of each semicircle decreases with the decrease in MgO content.

Table 3. Resistivity activation energies of the grain (E_g), extra arc (E_{ex}) and grain boundary (E_{gb}) semicircles (numbers given in parentheses are the corresponding regression coefficients)

Specimen	E_g *(kJ mol^{-1})*	E_{ex} *(kJ mol^{-1})*	E_{gb} *(kJ mol^{-1})*
ZM1	43·5 (0·999)	65 (0·999)	45·3 (0.982)
ZM2	78·1 (0·999)	73·3 (0·998)	57 (0·997)
ZM3	78·1 (0·999)	86 (0·999)	78·1 (0·999)
ZM4	83 (0·999)	89 (0·999)	94·5 (0·999)
ZM5	105 (0·999)	112 (0·999)	116 (0·999)
ZM6	126 (0·999)	—	141 (0·999)

A curious result must be stressed here. The variations of the grain resistivity are relatively small despite the important variations in concentration in the conducting phases (refer to the variations in the fraction V_m of the monoclinic phase in Table 2). Figure 12(a) shows that in the intermediate range of MgO compositions the grain resistivity is even approximately independent of the MgO concentration. For the extreme concentrations (ZM1 on one side and ZM5 on the other), the activation energies vary significantly [Fig. 12(b)], but the orders of magnitude of the resistivities do not differ greatly. The relatively large variations of the d.c. resistivities reported above (Fig. 6) are in fact mostly due to the important changes in the extra arc magnitude.

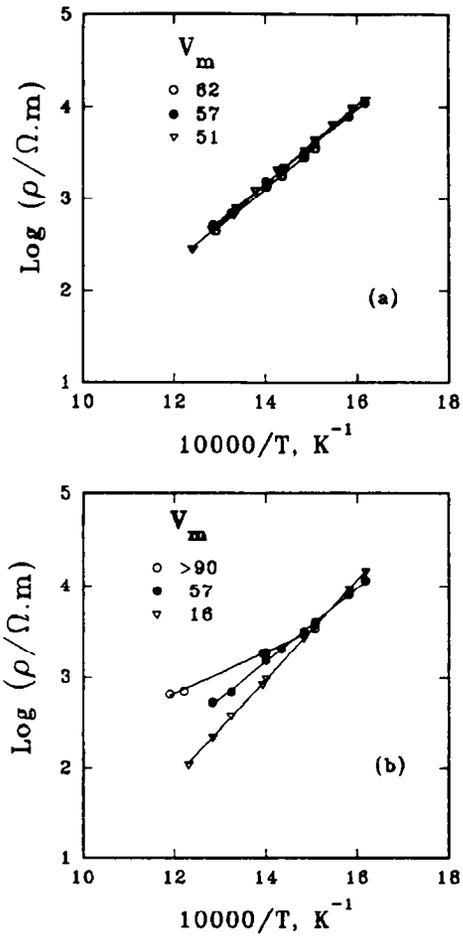

Fig. 12. Arrhenius diagrams of grain resistivities: (a) intermediate MgO contents; (b) extreme MgO contents.

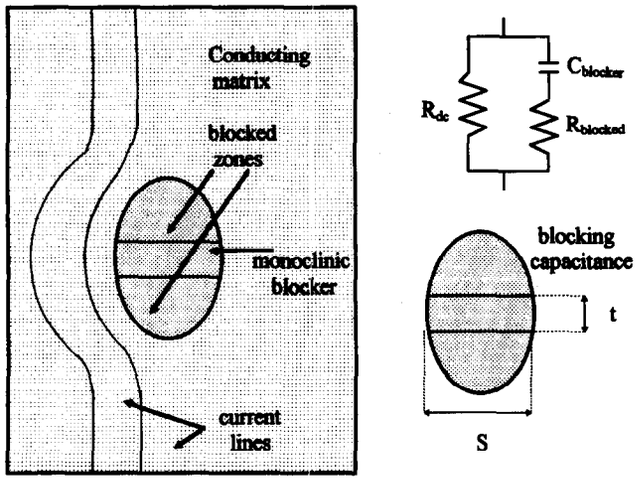

Fig. 13. Basic diagram of blocking process.

Most of our results show a strong analogy in electrical behaviour between the investigated Mg-PSZ and Al_2O_3–YSZ composites previously investigated.[20] This could indicate that the monoclinic grains in the Mg-PSZ materials mostly act as insulator grains. For the blocking process in the Al_2O_3 composites, a simple model summarized in Fig. 13 has been put forward.[20] In accordance with this model, the extra arc will be viewed as the response of a blocked *RC* circuit in which the capacitance *C* is associated with an 'average' isolating grain of monoclinic zirconia of area *S* and thickness *t*. Accordingly,

$$C = \epsilon\epsilon^0 S t^{-1}$$

where ϵ^0 and ϵ are, respectively, the vacuum permittivity and the relative permittivity of monoclinic zirconia. The resistance *R* stands for the part of the conducting matrix blocked by the capacitance (in a sort of space charge). Its volume is assumed to be approximately proportional to the blocker surface area *S* and its thickness approximately constant at a given temperature. It can be written as:

$$R \propto \rho S^{-1}$$

where ρ is the conducting matrix resistivity. According to the above equations, the relaxation frequency of the extra arc obeys the equation:

$$f_{ex} = (2\pi R\, C)^{-1}$$

or

$$f_{ex} \propto (\epsilon\epsilon^0 \rho\, t^{-1})^{-1}$$

The fact that the resistance and relaxation frequency associated with the blocking process usually exhibit activation energies very close to that of the matrix resistivity ρ, in agreement with the above equations, strongly supports the assumptions.

For verification and application of this simple model, two specific parameters have been defined:[26] the blocking factor α_R which measures the fraction of electric carriers being blocked by the blockers, and the frequency factor α_F. The blocking factor should be proportional to the overall area of the blocker cross-sections perpendicular to the electric field. The frequency factor should be proportional to the average blocker thickness and to the material permittivity. These correlations have been verified[23] with pores and voids in YSZ. The equation correlating α_F to the blocker thickness has even been numerically standardized. Steil *et al.*[20] give the following formula:

$$\alpha_F = 7{\cdot}8 \times 10^{-3}\epsilon t$$

where *t* is the average blocker thickness, in μm.

According to the model, the above specific parameters α_R and α_F should be calculated from the admittance diagrams of the results. Because of high overlapping in our diagrams and more difficult resolution in the admittance representation, we used impedance diagrams to determine α_R and α_F. This may have introduced some errors in the calculated values.

The first feature to be verified to ascertain the validity of this simple model is the independence of α_R and α_F with respect to the measurement conditions. Figures 14 and 15 show typical variations of these parameters with the measurement temperature for an intermediate composition (ZM4 sample). The measured parameters are not fully independent with respect to *T*, but the variations remain small. This corresponds to the close parallelism mentioned above between the grain and blocking processes relaxation frequency and resistivity Arrhenius diagrams.

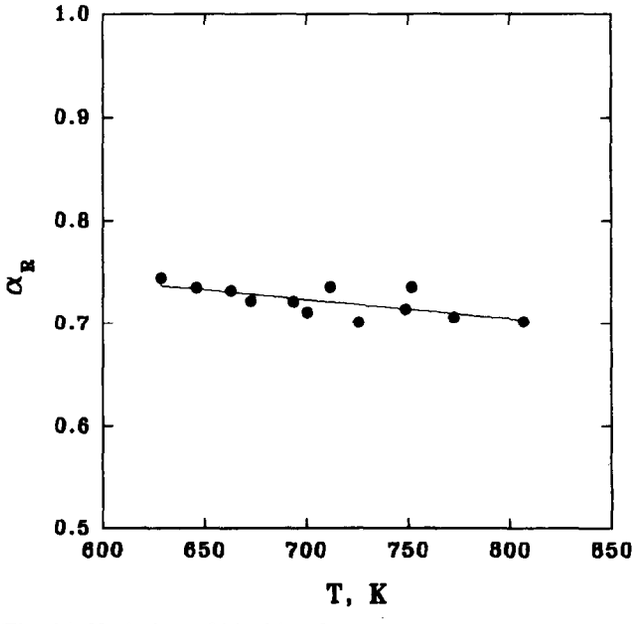

Fig. 14. Variation of blocking factor α_R with temperature for ZM4 sample.

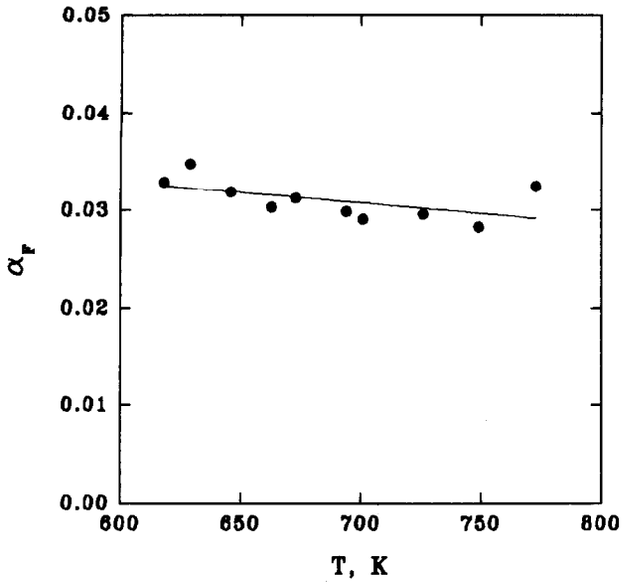

Fig. 15. Variation of frequency factor α_F with temperature for ZM4 sample.

From the average value of α_F calculated from the data in Fig. 15, and applying the previous equation, we calculated an average diameter of 4 μm for the monoclinic grains. This is in fairly good agreement with the micrographic observations. A similar calculation applied to the pores of 0·5 μm indicates that the corresponding relaxation frequency is about 100 times smaller than f_{ex}. This is a further argument supporting the assumption that the extra semicircle is mostly associated with the monoclinic grains.

Figure 16 shows the variations of the blocking factor with the monoclinic zirconia content V_m in our Mg-PSZ samples. As expected, α_R markedly increases with V_m. Despite large heterogeneities in the samples and significant uncertainties in the diagram resolutions, the scatter in the experimental results remained small and the agreement with the matrix-conduction–blocking model is reasonably good.

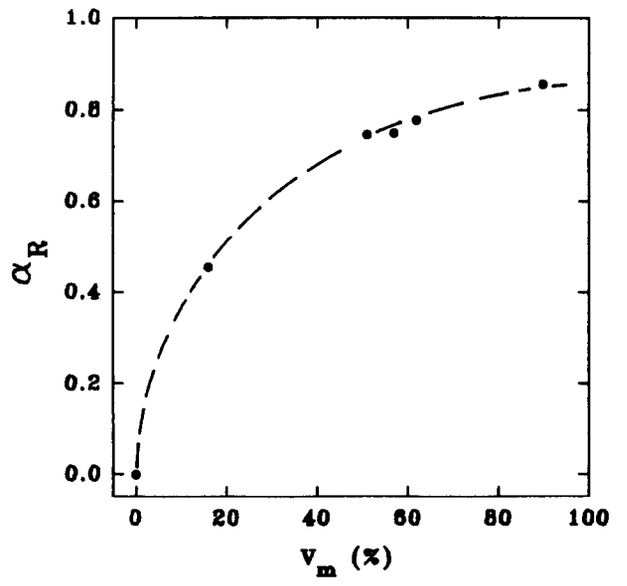

Fig. 16. Variation of blocking factor with monoclinic volume fraction V_m. T = 500°C.

5 Electrical Properties of Nominally Pure Zirconia

Another straightforward interpretation can be envisaged for the extra arc. It is sketched in Fig. 17. It assumes that the complex network of the conducting and monoclinic grains are electrically equivalent to two circuits in series describing, respectively, the electrical behaviours of the conducting grains (cubic and tetragonal) and the monoclinic grains. Interpretations of this type are frequently adopted to explain the grain boundary effects.[24]

Before entering into the details of our experimental results, let us recall an essential feature which is useful in solid state impedance spectroscopy. With a sufficiently 'simple' sample geometry and at a frequency sufficiently low for the skin effect to remain negligible, the sample resistance can be written as:

$$R = \rho k$$

where k is its geometrical factor; and its capacitance as:

$$C = \epsilon\epsilon^0 k^{-1}$$

Accordingly, the specific relaxation that we will determine by impedance measurements on the sample, is given by the equation:

$$f_{rel} = (2\pi\, \epsilon\epsilon^0)^{-1}$$

It is a specific property of the material, independent of the geometrical factor of the sample, and should be the same for a cubic sample and a grain

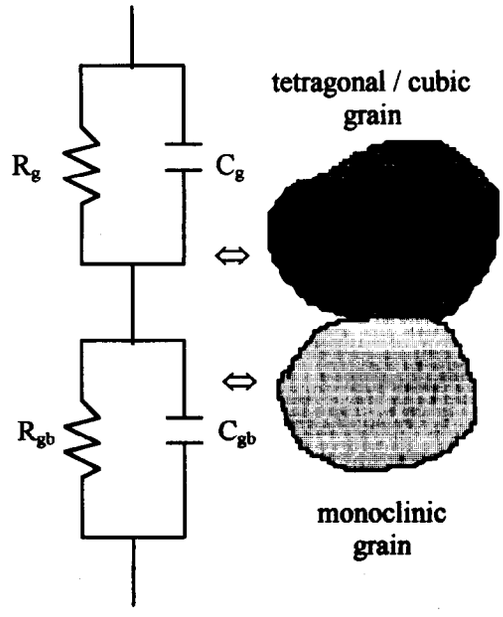

Fig. 17. Series model.

in a sintered material. It may be thought of as the signature of the material. Relaxation frequency measurements are therefore an easy test to identify a semicircle. In composite materials the electrical behaviours are slightly more complicated[20] because of interference between the components, especially related to the contribution of both components to the relative permittivity which determines the conducting grain relaxation.[20] However, this identification technique can still be used with appropriate adjustments.

To check the above assumption, impedance measurements were carried out on the NPZ samples prepared with the two pure zirconia powders (see Experimental Procedures section). They gave very similar results. All the recorded diagrams are essentially composed of a dominant bulk semicircle (Fig. 18) and a small low frequency arc which will not be examined in the following. The Arrhenius diagrams of the corresponding resistivity and relaxation frequency are shown in Figs 19(a) and 19(b), respectively. These experimental values should be regarded as approximate, because of the high porosity of the samples. For our purposes, only the orders of magnitude of these parameters are important (referring to a recent investigation of porous YSZ,[27] alteration factors of about 0·5 and 50 can be anticipated, respectively, for the permittivity and resistivity but with no major changes in the corresponding variations with temperature, especially in the resistivity activation energy).

The relaxation frequencies of monoclinic zirconia measured here are far lower than the values measured for the extra semicircles. For example, at 500°C, the monoclinic phase value is 51 Hz and those of the extra arc are in the 6·3–61 kHz range.

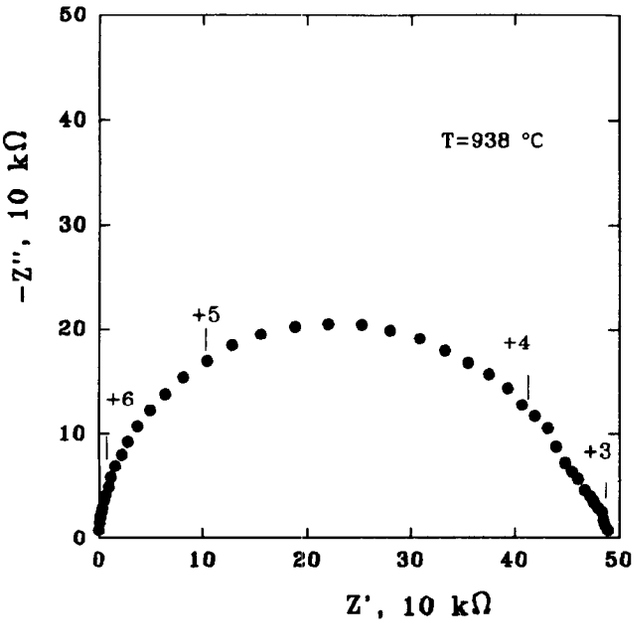

Fig. 18. Typical impedance diagram of monoclinic zirconia for NPZ sample.

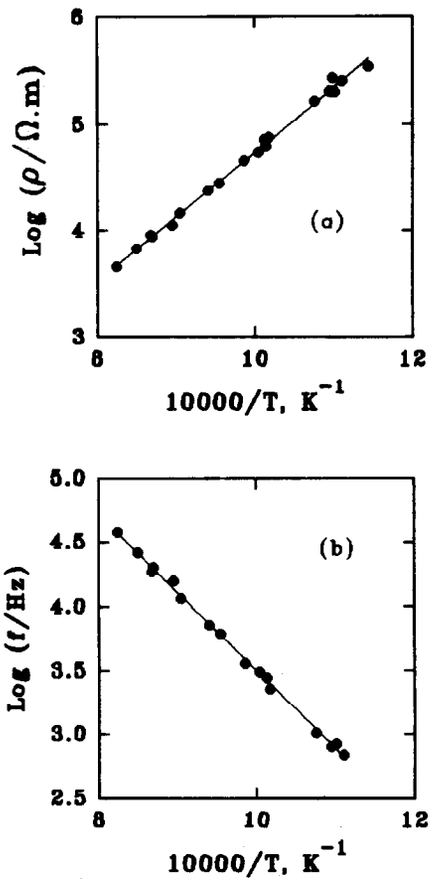

Fig. 19. Arrhenius diagram of resistivity (a) and relaxation frequency (b) of monoclinic zirconia in the 600–950°C temperature range for NPZ sample.

The resistivity activation energies also point to marked differences. The calculated value for the monoclinic phase is 118 kJ mol^{-1} in the 600–950 °C temperature range. For the extra arc, the calculated activation energies are all significantly smaller (see Table 3). Furthermore, the extra arc activation energy is variable and markedly depends on the MgO content. The assumption of the extra arc describing the specific electrical properties of the monoclinic grains can clearly be rejected.

6 Electrical Observation of the m ↔ t Phase Transformation of Nominally Pure Zirconia

We took advantage of the availability of these monoclinic samples to observe the reversible m↔t phase transformation also. Impedance measurements were carried out at various temperatures between 800 and 1370°C.

In the high-temperature range (>1000°C), the NPZ diagram looks like a regular zirconia conducting phase diagram (Fig. 20). As above, only the high-frequency semicircle, which describes the specific properties of the grains, is taken into consideration here. Figure 21 shows the corresponding resistivities measured during the cooling cycle.

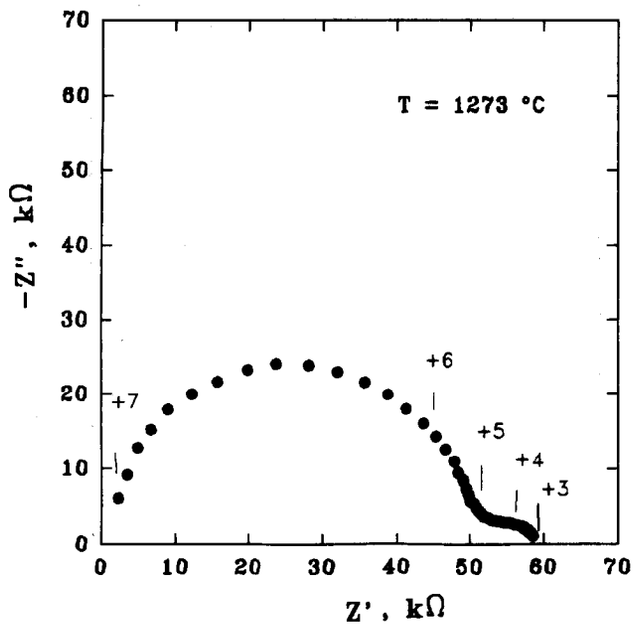

Fig. 20. Impedance diagram of tetragonal zirconia for NPZ sample.

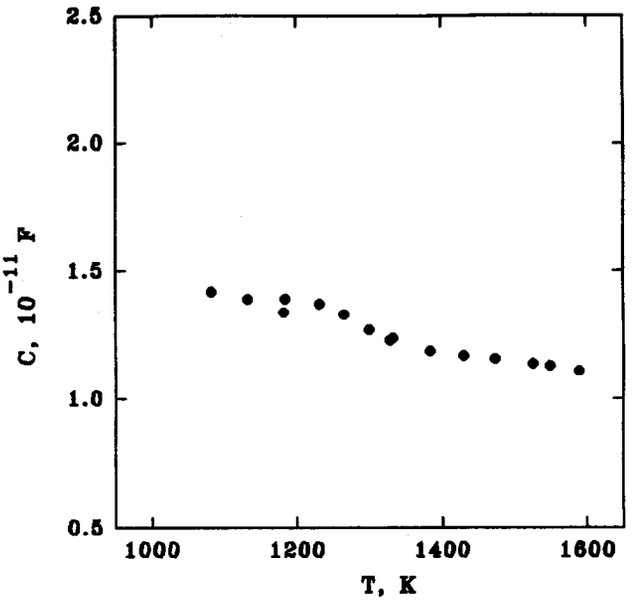

Fig. 22. Capacitance variations of pure zirconia sample (NPZ).

As expected, the plot exhibits two straight lines describing the variations of the tetragonal phase conductivity, at high temperature, and those of the monoclinic phase conductivity at low temperature. The activation energies calculated from these lines are 91 and 118 kJ mol^{-1}, respectively, for the tetragonal and monoclinic phases.

The width of the temperature range over which the transition occurs is ~170 °C, in fair agreement with earlier d.c. measurements.[25] The points obtained in this temperature range of 'athermal' transition correspond to steady-state conditions. As a check, measurements were also performed after 15 h of annealing. The results marked by filled circles on the plot (Fig. 21) are perfectly aligned with the others which were more rapidly obtained.

From the impedance semicircles, the sample capacitances have also been determined. Since the effect of the sample porosity is likely to be constant and the permittivity to remain proportional to the measured capacitances, the curve shown in Fig. 22 indicates that the tetragonal ↔ monoclinic phase change does not alter much the permittivity of pure zirconia. The absence of any significant strong variation in the transition range is another interesting result.

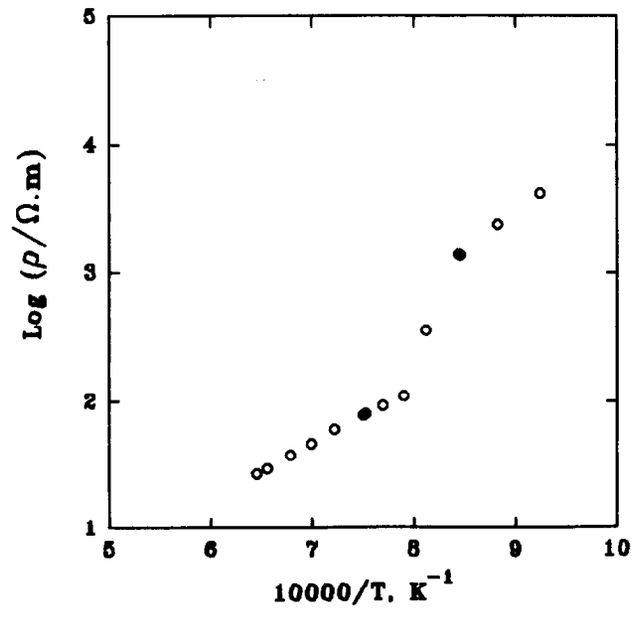

Fig. 21. Effect of t → m transformation on specific resistivity of pure zirconia for NPZ sample.

7 Phase Decomposition of Mg-FSZ and Mg-PSZ

On the basis of the reported observations, it was concluded that impedance spectroscopy can easily measure the blocking effect due to the presence of a monoclinic phase. Therefore, it should be an appropriate technique to quantitatively follow the destabilization of a conducting zirconia matrix. Destabilization annealings of Mg-FSZ and Mg-PSZ samples were carried out to confirm this assumption.

From several previous micrographic studies[8,9,11,12] on Mg-FSZ, it has been well established that during destabilization, the monoclinic phase is generated at grain boundaries. The cubic phase may crack because of a large difference in the thermal expansion coefficients of the c and m phases. After reaction completion, the observed microstructure usually consists of a fine-grained (1–5 μm) monoclinic phase containing thoroughly dispersed magnesia-rich pipes.

The compositions of the samples we investigated were 13·7 mol% (ZM6) and 8 mol% MgO (ZM4). The annealing temperature was 1100 °C and the annealing times 1, 2, 3, 4, 6, 8 and 14 h. At this temperature, a rather high decomposition rate is expected. In fact, no cubic phase reflections were observed by X-ray diffraction after 14 h annealing.

The destabilization of the material results in significant changes of the impedance diagram which affect all the semicircles. The diagrams were more easily analysed for the Mg-FSZ sample for which the initial diagram is simpler [see Fig. 5(a)]. The details below are given for this sample. After 1 h annealing, the impedance spectra is similar in shape to the original diagram. However, a more careful analysis shows that the grain boundary semicircle has more markedly changed. Besides the expected increase in the corresponding resistivity, the relaxation frequency has also increased. According to the model cited above, this can be interpreted in terms of simultaneous increases in the surface areas and the thicknesses of the growing monoclinic phase which still behaves as a grain boundary blocker. The depression angle also increases, indicating an increase in the heterogeneity of this grain boundary blocking effect. After 2 h annealing, the impedance diagram no longer exhibits the original shape, as shown in Fig. 23. Most likely, the monoclinic grains are already large enough to result in an extra arc with a relatively high relaxation frequency. The very large depression angle (38°) of the blocking semicircle and the relative increase in its relaxation frequency suggest the growth of another semicircle which overlaps with the true grain boundary arc. After this 'first stage', the overlaps become so

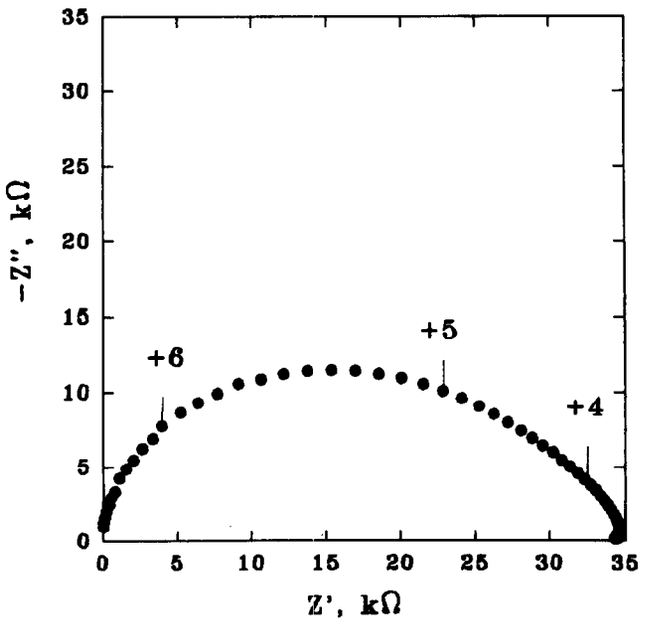

Fig. 23. Impedance diagram of ZM6 after 2 h annealing at 1100°C. Measuring temperature 553°C.

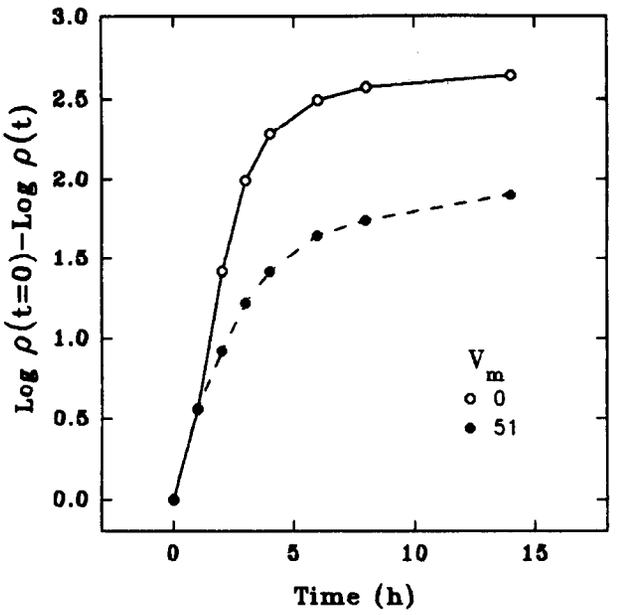

Fig. 24. Variations of ZM6 (○) and ZM4 (●) resistivities with annealing time. Annealing temperature 1100°C; measuring temperature 553°C.

strong among all the electrical responses, that it would not be realistic to envisage any semicircle separation. (The cracks that are known to be generated during the destabilization may also contribute to impedance diagram complexity.)

To quantitatively characterize the destabilization process, we simply determined the corresponding variations in the overall sample resistivity. The measurements were performed after temporarily cooling the samples to 553°C. For that, we measured the real impedance components at 10 kHz. We checked on the diagrams that this frequency approximately corresponds to the real intercept which includes the blocking effect (in other words, to the d.c. resistance). Figure 24 shows that the resistivities of the ZM6 and ZM4 samples increase very fast at a 1100°C annealing temperature. From these impedance results, it can be estimated that after 3 h at 1100°C, the d.c., resistivities have approximately increased by a factor of 100. Both samples behave similarly. After the 14 h annealing time, a steady-state situation seems to be reached which probably corresponds to a full transformation of the conducting phases into the monoclinic phase.

Table 4 compares the resistivites at 553°C

Table 4. Resistivity values at 553°C and activation energies of samples containing mostly monoclinic zirconia

Specimen	ρ *(Ωm)*
Annealed ZM6	$2{\cdot}13 \times 10^4$
Annealed ZM4	$2{\cdot}84 \times 10^4$
NPZ	$1{\cdot}62 \times 10^6$
ZM1	$6{\cdot}24 \times 10^2$

obtained under these conditions to that of the true monoclinic zirconia (NPZ sample) and to that of a material (ZM1 sample) which contains ~90% monoclinic zirconia. The resistivity of the monoclinic ZM6 and ZM4 materials and that of the nominally pure zirconia differ significantly and the difference is too large to be explained in terms of porosity effects. This may indicate that the MgO solubility in the monoclinic phase is not nil and that dissolved MgO induces a noticeable decrease in its resistivity or that the complex microstructure of the destabilized materials strongly influences their resistivities.

The ZM1 sample also behaves differently, with a much lower resistivity. This clearly indicates that even at its composition (with ~90% monoclinic phase), the electrical behaviour of the material is still dominated by the conducting grains present in it. A similar observation was made with Al_2O_3–YSZ composites[20] which show the characteristic features of YSZ up to more than 70% Al_2O_3.

8 Conclusions

In terms of electrical behaviour, the monoclinic grains in partially stabilized zirconias mostly act as an insulating second phase. There is no sharp discontinuity at the cubic phase limit. As the MgO content decreases below this limit, the main effect is a gradual increase in the blocking process due to the increasing population of monoclinic grains. As observed with other zirconia-based systems, the activation energy of the conducting phase (or the mixture of the conducting phases) markedly decreases with the MgO contents. Impedance spectroscopy is a powerful tool to study zirconia phase transformations and the destabilization processes.

Acknowledgements

The authors would like to express their appreciation to Zirconia Sales for providing the zirconia powder, to M. Hénault from the LIESG and to the research staff at IPEN for technical assistance. One of the authors (ENSM) also acknowledges CNPq/RHAE (process 260134/91.0) and FAPESP (process 92/2962-6) support.

References

1. Muccillo, E. N. S. & Kleitz, M., Ionic conductivity of fully stabilized ZrO_2: MgO and blocking effects. *J. Eur. Ceram. Soc.*, **15** (1995) 51–5.
2. Subbarao, E. C., Zirconia, an overview. In *Advances in Ceramics, Vol. 3: Science and Technology of Zirconia I*, eds A. H. Heuer and L. W. Hobbs. American Ceramic Society, Columbus, OH, 1981, pp. 1–24.
3. Hannink, R. H. J. & Garvie, R. C., Sub-eutectoid aged Mg–PSZ alloy with enhanced thermal up-shock resistance. *J. Mater. Sci.*, **17** (1982) 2637–43.
4. Wen, T. L., Li, N. X., Kuo, C. & Weppner, W., Conductivity of MgO-doped zirconia. *Solid State Ionics*, **18/19** (1986) 715–19.
5. Poulsen, F. W., Sorensen, J. B. B., Ahari, K. G., Knab, G. G. & Hartmanova, M., Oxygen ion conduction in ternary zirconia mixtures: effect of SrO on MgSZ. *Solid State Ionics*, **40/41** (1990) 947–51.
6. Viechnicki, D. & Stubican, V. S., Mechanism of decomposition of the cubic solid solutions in the system ZrO_2–MgO. *J. Am. Ceram. Soc.*, **48** (1965) 292–7.
7. Swain, M. V., The effect of decomposition on the thermal shock behaviour of Mg–CSZ. *J. Mater. Sci. Lett.*, **2** (1983) 279–82.
8. Hannink, R. H. J., Microstructural development of sub-eutectoid aged MgO–ZrO_2 alloys. *J. Mater. Sci.*, **18** (1983) 457–70.
9. Swain, M. V., Garvie, R. C. & Hannink, R. H. J., Influence of thermal decomposition on the mechanical properties of magnesia-stabilized cubic zirconia. *J. Am. Ceram. Soc.*, **66** (1983) 358–62.
10. Lamon, J., Thorel, A. & Broussaud, D., Influence of long-term ageing upon the mechanical properties of partially stabilized zirconia (Mg–PSZ) for heat-engine applications. *J. Mater. Sci.*, **21** (1986) 2277–82.
11. Farmer, S. C., Heuer, A. H. & Hannink, R. H. J., Eutectoid decomposition of MgO-partially stabilized ZrO_2. *J. Am. Ceram. Soc.*, **70** (1987) 431–40.
12. Porter, D. L. & Heuer, A. H., Microstructural development in MgO-partially stabilized zirconia (Mg–PSZ). *J. Am. Ceram. Soc.*, **62** (1979) 298–305.
13. Paulus, M., The influence of powder synthesis techniques on processes occurring during compact formation and its sintering. In *Materials Science Research, Vol. 17: Emergent Process Methods for High-Technology Ceramics*, eds R. F. Davis, H. Palmour III and R. L. Porter. Plenum Press, New York, 1984, pp. 177–91.
14. Ioffe, A. I., Rutman, D. S. & Karpachov, S. V., On the nature of the conductivity maximum in zirconia-based solid electrolytes. *Electrochim. Acta*, **23** (1978) 141–2.
15. Badwal, S. P. S., Effect of dopant concentration on electrical conductivity in the Sc_2O_3–ZrO_2 system. *J. Mater. Sci.*, **22** (1987) 4125–32.
16. Schouler, E., Kleitz, M. & Deportes, C., Applications selon Bauerle du tracé des diagrammes d'admmittance complexe en eléctrochimie des solides. II – Etude de la conductivité de la zircone stabilisée à l'yttrium. *J. Chim. Phys.*, **9** (1973) 1309–16.
17. Stratton, T. G., Reed, D. & Tuller, H. L., Study of boundary effects in stabilized zirconia electrolytes. In *Advances in Ceramics, Vol. 1: Grain Boundary Phenomena in Electronic Ceramics*, eds L. M. Levinson. American Ceramic Society, Columbus, OH, 1981, pp. 114–23.
18. Janke, D. & Fischer, W. A., Elektrische eigenschaften oxidkeramischer festelektrolyte bei stahlschelz-temperaturen. *Arch. Eisenhüttenwes*, **48** (1977) 311–18.
19. Kleitz, M., Bernard, H., Fernandez, E. & Schouler, E., Impedance spectroscopy and electrical resistance measurements on stabilized zirconia. In *Advances in Ceramics, Vol. 3: Science and Technology of Zirconia I*, eds. A. H. Heuer and L. W. Hobbs. American Ceramic Society, Columbus, OH, 1981, pp. 310–36.
20. Steil, M. C., Thévenot, F., Dessemond, L. & Kleitz, M., Impedance spectroscopy analysis of conduction percolation in zirconia–alumina composites. In *Proceedings of 3rd European Ceramic Society Conference*, eds P. Duran and J. F. Fernandez. Faenza Editrice Iberica SL, San Vicente, 1993, pp. 271–80.
21. Cormack, A. N. & Parker, S. C., Some observations on the role of dopants in phase transitions in zirconia from

atomistic calculations. *J. Am. Ceram. Soc.*, **73** (1990) 3220–4.
22. Dessemond, L., Muccillo, R., Hénault, M. and Kleitz, M., Electric conduction–blocking effects of voids and second phases in stabilized zirconia. *Appl. Phys.*, **A57** (1993) 57–60.
23. Kleitz, M., Pescher, C. & Dessemond, L., Impedance spectroscopy of microstructure defects and crack characterization. In *Zirconia V: Science and Technology of Zirconia*, eds S. P. S. Badwal, M. J. Bannister and R. H. J. Hannink. Technomic Publishing Co., Lancaster, 1992, pp. 593–608.
24. Chu, S. H., Seitz, M. A., J., The a.c. electrical behavior of polycrystalline ZrO_2: CaO. *J. Solid State Chem.*, **23** (1978) 297–314.
25. Subbarao, E. C., Maiti, H. S. & Srivastava, K. K., Martensitic transformation in zirconia. *Phys. Stat. Sol. (a)*, **21** (1974) 9–40.
26. Dessemond, L., Spectroscopie d'impédance des fissures dans la zircone cubique. Thesis, Grenoble, November 1992.
27. Kleitz, M., Dessemond, L., Steil, M. C., Effects of pores, inclusions and cracks on the ionic conduction in YSZ, 22d Meeting of the Japanese Solid Oxide Fuel Cells Society, Yokohama, March 1994.